# NUMERICAL SIMULATION FOR DETERMINATION OF TEMPERATURE FIELD AND RESIDUAL STRESS OF STAINLESS STEEL BUTT JOINTS WITH AND WITHOUT CLAMPING

**Nguyen Tien Duong**

*School of Mechanical Engineering, Hanoi University of Science and Technology,
No. 1 Dai Co Viet Street, Hai Ba Trung, Ha Noi, Viet Nam*

Emails: *duong.nguyentien@hust.edu.vn*

**Abstract.** Many welded structures are fabricated from stainless steels because these steels have good mechanical properties and good corrosion resistance. It is necessary to predict the residual stress after welding in order to evaluate the performance of the welded joint. In this paper, the butt welded joint of AISI 316L stainless steel plates is studied. The Metal Inert Gas (MIG) welding process is selected for this material. A SYSWELD software based on the Finite Element Method (FEM) is used to determine the temperature field and residual stresses of two stainless steel plates. The welding simulation includes a sequential coupled thermomechanical analysis. The elemental generation and death technique is utilized to simulate metal deposition in welding. The double ellipsoidal heat source model is used for the heat input of the MIG welding process. The temperature distribution for various time steps at some important points is presented. Cooling times and cooling rates over a temperature range of 800 $^{\circ}$C to 500 $^{\circ}$C at these points are determined. The residual stress distribution in the longitudinal and transverse direction in two cases with and without clamping is obtained and compared. Obtained results show that: the temperature field in the case of clamping is the same as in the case of no clamping; only the longitudinal stress and transverse stress components are important, the other stress components are not important; the longitudinal stress at the middle of weld line is very high; the transverse stress in the case of clamping is greatly increased, so it is necessary to limit clamping to reduce residual stress after welding.

*Keywords:* butt joint, finite element, MIG welding, residual stress, stainless steel.

*Classification numbers*: 5.1.1, 5.1.4.

## 1. INTRODUCTION

Stainless steels are resistant to corrosion. They have strength at elevated temperatures, toughness at low temperatures. So they are used in many sectors: pharmaceuticals, building materials in large buildings, paper factories, chemical plants, water treatment factories, components of heat exchangers and chemical reactors, storage tanks and tankers (for oil, chemicals, and foodstuffs), pressure vessels, etc. The most commonly used stainless steel is austenitic grade 316L. The weldability of grade 316L is very good, but it is necessary to choose

a suitable welding process. Gas Metal Arc Welding (GMAW) process is a clean and cost effective process in arc welding, offering higher productivity and good quality. The GMAW process with inert gas, called MIG (Metal Inert Gas) welding, is most suitable for stainless steels [1]. Automatic MIG welding provides precise control of the welding procedure for better weld quality.

Fusion welding in general and MIG welding in particular produce a high residual stress field. In welding, the residual stress field is created due to non-uniform heating and cooling. This residual stress field, combined with the stresses resulting from service loads, strongly affects the serviceability and service life of the welded structure. We need to predict residual stresses to evaluate the load capacity and life of structures.

It is reasonable to apply numerical methods in order to avoid expensive experimental measurements. The finite element method is the most commonly used numerical method to solve thermomechanical problems in welding. First, a transient heat transfer analysis is used to calculate the temperature history at all nodes. Then, this thermal loading is used to determine displacement, strain and stress by a static mechanical analysis. Each step of the mechanical analysis corresponds to a time step in the thermal analysis. The restrained thermal expansion causes the development of plastic strains. Finally, at the last step, when the temperature reaches its initial value, the residual stress field is obtained as a result of all intermediate analysis steps.

Many softwares based on finite element method (FEM) have been developed for stress and strain analysis in structures such as ABAQUS, ANSYS, NASTRAN, MARC, SYSWELD, etc. [2 - 5], of which SYSWELD [3, 6] was developed specifically for welding and heat treatment.

This paper uses SYSWELD software to simulate and determine residual stresses and strains in a butt welded joint of stainless steel. It is a butt joint of two plates that have the same dimensions as 500 mm (length) × 200 mm (width) × 5 mm (thickness). The automatic MIG welding process is applied. Both base material and filler metal are AISI 316L stainless steel. The temperature field during welding is obtained by thermal analysis. Cooling times and cooling rates over a temperature range of 800 $^{\circ}$C to 500 $^{\circ}$C at some important points are determined. This is the temperature range where changes in the structure and properties of metal materials occur. Calculation of residual stresses and welding strains is performed in two cases: without clamping and with clamping at the edge of the two sides. The element birth and death technique is used to simulate the variation of deposited metal over time in a butt weld. The heat source model for MIG welding process is a double ellipsoidal form.

## 2. NUMERICAL MODELING BY FINITE ELEMENT METHOD

Welding simulation was considered a sequentially coupled thermomechanical analysis and the element birth and death technique was used to simulate the deposition of filler metals. The thermal analysis is solved independently of the mechanical analysis. The connection between the thermal and mechanical analysis is obtained through temperature history. First, a transient thermal analysis is implemented during which the time-dependent temperature distribution is calculated for the successive build-up of the welding pass. The temperature field at each time step is then used as input data for evaluating the displacement, strain and stress in welded joints.

The determination of temperature field and the calculation of residual stress are performed using SYSWELD finite element software. In the element birth and death technique, at the beginning, a finite element mesh of the welded joint including the base material and deposition material is generated. Subsequently, all weld elements are deactivated (element death) in the thermal analysis and their conductivity is assigned to a number close to zero. When the heat

input is supplied, the weld elements are reactivated (element birth) and their conductivity is reset to the original value. Similarly, in the mechanical analysis, the weld elements are firstly deactivated and their stiffness is assigned to a number close to zero. When the elements are reactivated, their stiffness is reset to the original value again. The same finite element mesh and time increments were used for both thermal and structural analysis.

Thermal analysis is performed to determine the temperature distribution in the welded plates. The governing differential equation for transient heat transfer during welding in an isotropic material is given in the form of:

$$\rho c \frac{\partial T}{\partial t} = \lambda \left( \frac{\partial^2 T}{\partial x^2} + \frac{\partial^2 T}{\partial y^2} + \frac{\partial^2 T}{\partial z^2} \right) + q \tag{1}$$

where $T$ is the transient temperature at the point $(x, y, z)$ at time $t$; $q$ is the internal heat source; $\rho$, $c$, $\lambda$ are the material density, specific heat capacity and thermal conductivity, respectively.

The double semi-ellipsoidal heat source model used in the numerical simulation is proposed by Goldak. The double ellipsoidal heat source model is shown in Figure 1.
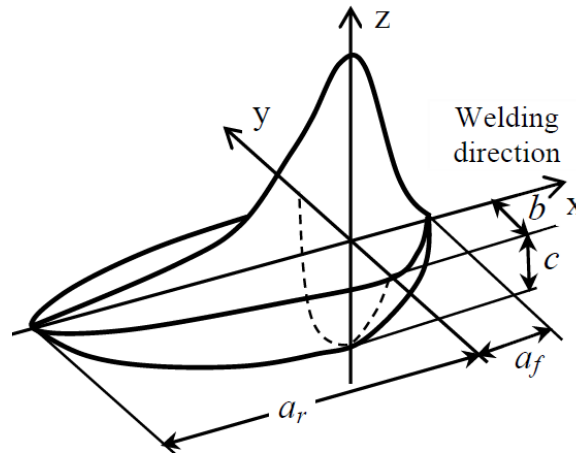


*Figure 1.* Double ellipsoidal heat source model application in T-joint welds.

The heat source distribution in the front part of the ellipsoid has the following form:

$$q_f(x, y, z) = \frac{6\sqrt{3} f_f Q}{a_f bc \pi \sqrt{\pi}} \exp \left( -\frac{3x^2}{a_f^2} - \frac{3y^2}{b^2} - \frac{3z^2}{c^2} \right) \tag{2}$$

The formula of the heat source distribution in the rear part of the ellipsoid is:

$$q_r(x, y, z) = \frac{6\sqrt{3} f_r Q}{a_r bc \pi \sqrt{\pi}} \exp \left( -\frac{3x^2}{a_r^2} - \frac{3y^2}{b^2} - \frac{3z^2}{c^2} \right) \tag{3}$$

where Q is the power input:

$$Q = \eta.U.I$$

here $\eta$ represents the heat input efficiency; $U$ is the welding potential; $I$ is the welding current.

$a_f$, $a_r$, $b$ and $c$ (Figure 1) are related to the geometry of heat source for the welding being modeled. The values of $a_f$, $a_r$, $b$ and $c$ are determined by direct measurement of weld pool geometry through experimentation; $f_f$ and $f_r$ are proportion coefficients representing heat apportionment in front and behind the heat source, respectively, $f_f + f_r = 2$. The values for these two coefficients are calculated as follows [8]:

$$f_f = 2a_f / (a_f + a_r) \tag{4}$$

$$f_r = 2a_r / (a_f + a_r) \tag{5}$$

The finite element meshes in the mechanical analysis are the same as those in the thermal analysis. The temperature history determined in the thermal analysis is imposed as a temperature load at each time step in the mechanical analysis. The total strain increment $d\varepsilon$ at the integration point as a function of elastic strain, plastic strain and thermal strain is given by the following equation:

$$d\varepsilon = d\varepsilon^E + d\varepsilon^P + d\varepsilon^T \tag{6}$$

where $d\varepsilon^E$, $d\varepsilon^P$ and $d\varepsilon^T$ are the elastic, plastic and thermal strain increments, respectively.

In this study, a 3D finite element model is constructed. A fine mesh is used in zones near the weld line and a coarser mesh is used in regions away from the welding zone. The most appropriate model for the heat source for MIG welding process is to use the double ellipsoidal heat source [3]. The parameters for heat source model used in SYSWELD for this study are adjusted by experiment on the welding sample. When the weld geometry and sizes obtained by modeling are in good agreement with those of the experiment, it gives the final double ellipsoid parameters.

At the starting of weld line, the heat transfer is fast due to the low temperature of workpices. So, the input heat needs to be higher than that in the middle of weld line in order to ensure the penetration at the starting of weld line. While at the termination of weld line, there is a risk of burning through the weld due to very high temperature, the heat input must be reduced. In SYSWELD simulation, these problems are solved by energy factor. It means that the coefficient of the heat source is multiplied by a factor greater than 1.0 at the starting of weld line and it is multiplied by a factor less than 1.0 at the termination of weld line.

## 3. APPLICATION

In this study, AISI 316L stainless steel plates with 5.0 mm thickness are welded using an automatic MIG welding process. The material of deposited metal is the same as the base material. The composition of the sample is shown in Table 1 [9].

*Table 1*. Chemical compositions (wt. %) of AISI 316L stainless steel.

| C | Mn | Si | P | S | Cr | Ni | Mo | Cu |
|------|-----|-----|-------|------|------|------|-----|-----|
| 0.03 | 2.0 | 0.5 | 0.025 | 0.01 | 18.0 | 12.5 | 2.7 | 0.3 |

AISI 316L stainless steel has physical properties such as: elastic modulus E = 195 (Gpa), density $\rho$ = 8 (g/cm$^3$), coefficient of thermal expansion $\alpha$ = 16.6 $\times$ 10$^{-6}$ (1/$^0$C), thermal conductivity 15.7 w/mk, convective heat transfer coefficient 10 W.m$^{-2}$.$^o$K$^{-1}$, and melting point $T_m$ = 1450 $^o$C [10]. The mechanical properties of this material are as follows: strength $\sigma_Y$ = 207

(Mpa), ultimate tensile strength $\sigma = 538$ (Mpa), elongation $\delta = 55$ % [10]. The material properties are dependent on temperature. The data bank in the SYSWELD software will provide the values of the parameters of this material at the considered temperature.

The two plates in butt welded joint have the same dimensions. The dimensions of each plate are 500 mm (length) × 200 mm (width) × 5 mm (thickness). The single Y groove is prepared with the following dimensions: the groove angle $\alpha = 60^\circ$, the root face f = 1.5 mm, and the root gap g = 1 mm (Figure 2). The weld is perfomed by one pass with the weld sizes: excess weld thickness e = 1 mm, penetration bead thickness p = 0.5 mm (Figure 2).
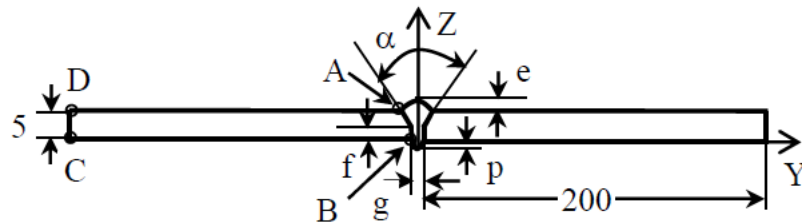


*Figure 2.* Joint dimensions and weld sizes.

The 3D elements in brick-type and triangular prism elements are selected. In order to reduce the time calculation by reducing the number of nodes and elements, the uneven meshing technique is constructed, whereby the areas of high temperature gradients in the weld line and its vicinity use a fine mesh and the zones away from the weld line have a coarser mesh. The finite element mesh is simulated with a total of 108008 finite elements and 88572 nodes (Figure 3). In both the thermal and mechanical analyses, the finite elements have the same mesh.

Analysis was performed using a 3D moving heat source in a double ellipsoidal model. The parameters for the heat source model are obtained by comparing simulation with experiment. First, initial values of the heat source parameters are supplied, and the simulation results are compared with the actual shape of weld pool on the welding specimens. Continuous adjustment is made so that the simulation results are consistent with the weld pool shape, and the accurate heat source model is obtained. The final values for heat source during MIG welding process in the SYSWELD model are 10 mm length, 6 mm width, and 5 mm penetration. These geometry parameters of heat source correspond to the symbols in Figure 1, we have:

$$a_f + a_r = 10 \text{ mm}; \ b = 6 \text{ mm}; \ c = 5 \text{ mm}.$$

The parameters at the begining of weld line are a ramp length of 10 mm and an energy factor of 1.1. The parameters at the termination of weld line are a ramp length of 10 mm and an energy factor of 0.8.

The welding parameters obtained by the adjustment of model data and experimental results must ensure the requirements of shape, size and quality, good penetration and without defects. Those parameters will be taken to simulate and determine residual stresses and welding strains. The values of welding parameters include welding current $I = 135$ (A), welding potential $U = 21$ (V), welding speed V = 4.5 (mm/s), and heat efficiency of welding arc $\eta = 0.85$.

The welding torch moves in a straight line along the welding direction. The velocity of heat source is equal to the welding speed. To determine residual stresses after welding, the specimen

is cooled to room temperature. The cooling method used was natural cooling over time. The initial temperature of specimens is equal to the ambient temperature (25 $^{\circ}$C).
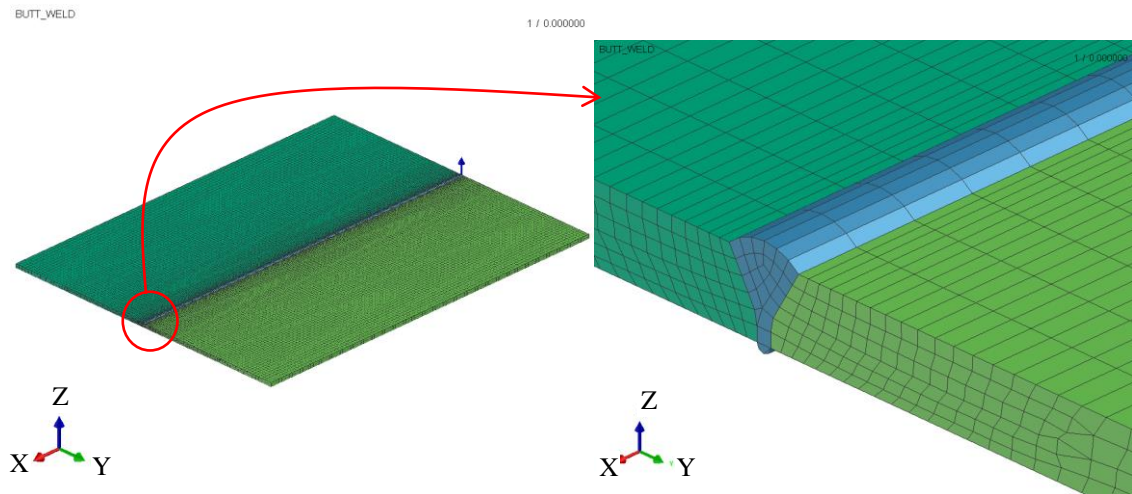


*Figure 3.* Finite element mesh in SYSWELD simulation.



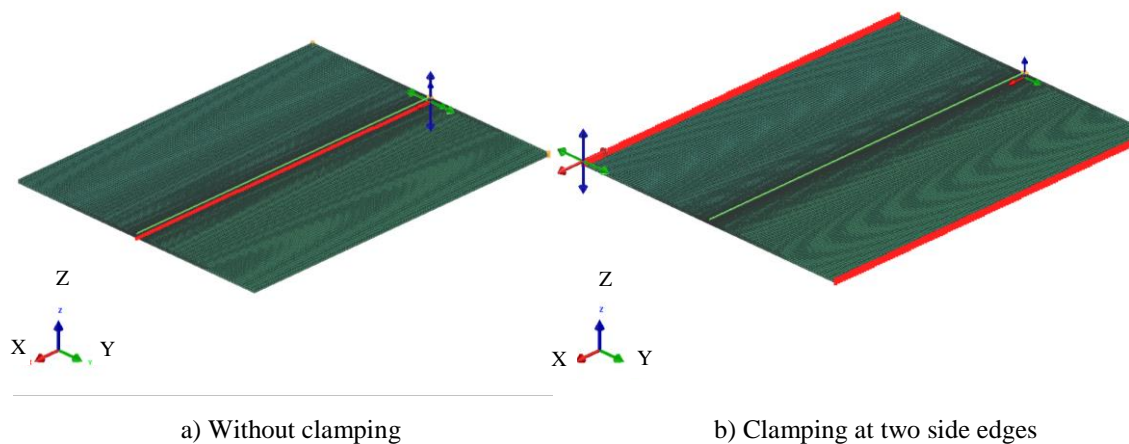a) Without clamping                    b) Clamping at two side edges

*Figure 4.* Boundary conditions.

Mechanical boundary conditions are considered in two cases:

- Case 1 - Without clamping (Figure 4a): due to the symmetry of the structure (two plates have the same width), at the position of weld line there is no displacement in the horizontal direction (in the OY axis) and the vertical direction (in the OZ axis). So, the displacement in 2 directions OY and OZ of all nodes on the weld line at the bottom of the plate is fixed.

- Case 2 - Clamping at two side edges (Figure 4b): the displacement in 3 directions OX, OY and OZ of all nodes on two side faces at both end edges is fixed.

## 4. RESULTS AND DISCUSSION

### 4.1. Temperature field

718

The obtained simulation results shows that there is no difference in temperature field in the two cases (without clamping and clamping at two end edges). The fusion depth on the top surface of the weld is 0.7 mm. It is 1.2 mm in the middle of the plate thickness. The fusion depth at the bottom surface of the weld is 0.6 mm. The weld has satisfactory shape and size, complete fusion, and enough penetration (Figure 5).

The temperature distribution for various time steps at the weld toe (Point A in Figure 2) in the center of weld line is presented in Figure 6. The maximum temperature at this point reaches 1839 $^o$C. This temperature is obtained after welding for 56.5 seconds. The temperature of this point cools to 800 $^o$C in 68 seconds and it drops to 500 $^o$C in 88.5 seconds. The cooling time from 800 $^o$C to 500 $^o$C at this point is 20.5 seconds. Thus, the cooling rate in the temperature range from 800 $^o$C to 500 $^o$C ($\Delta t_{8/5}$) is 14.6 ($^o$C/s). At the finishing of weld seam, the temperature at this point is still 384 $^o$C.



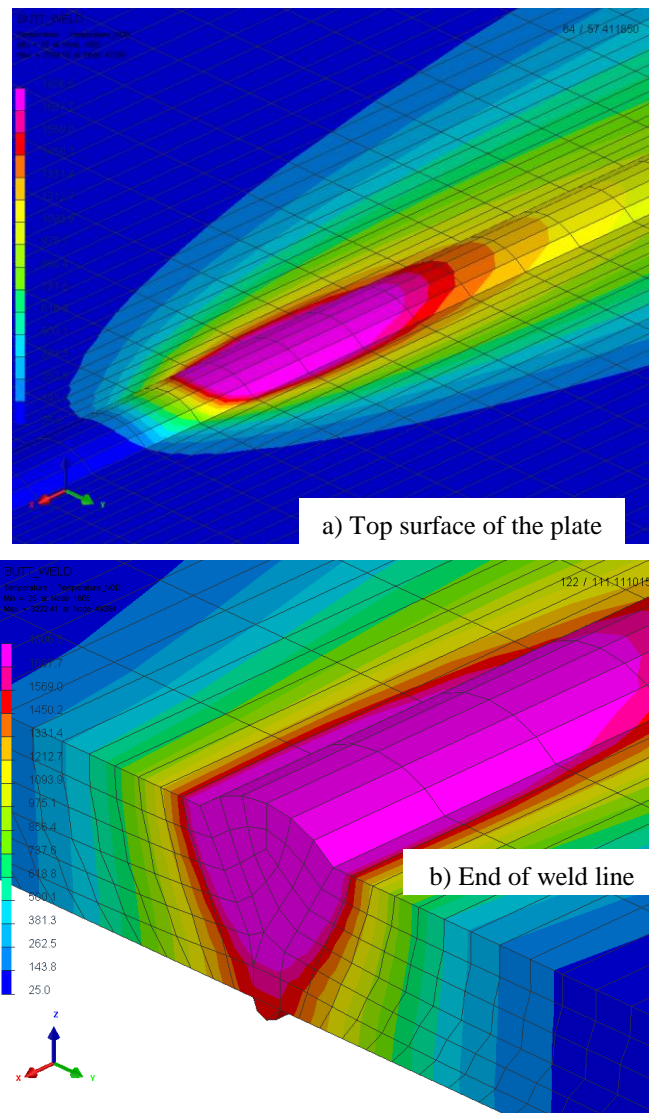a) Top surface of the plate



b) End of weld line

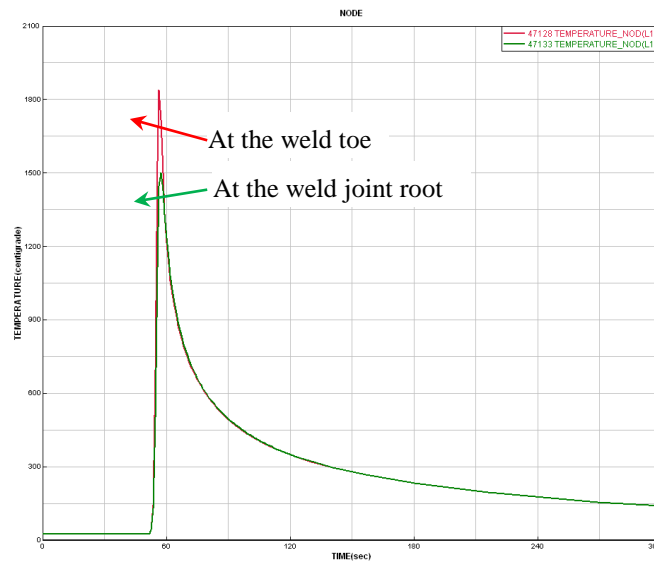*Figure 5.* Temperature field in butt welded joint.

*Figure 6.* Temperature distribution at the joint groove face.

The temperature distribution for various time steps at the weld joint root (Point B in Figure 2) in the center of weld line is given in Figure 6. The maximum temperature at this point is 1500.8 $^{o}$C. This temperature is obtained after welding for 57.4 seconds. This temperature is still higher than the melting point of the material (= 1450 $^{o}$C), so the joint root is guaranteed to melt and the weld is fully complete fusion. The cooling time from 800 $^{o}$C to 500 $^{o}$C at this point is 20 seconds. The cooling rate in the temperature range from 800 $^{o}$C to 500 $^{o}$C ($\Delta t_{8/5}$) is 15 ($^{o}$C/s). Thus, the cooling rate at this point is only slightly higher than the cooling rate at the weld toe (15 $^{o}$C/s versus 14.6 $^{o}$C/s).
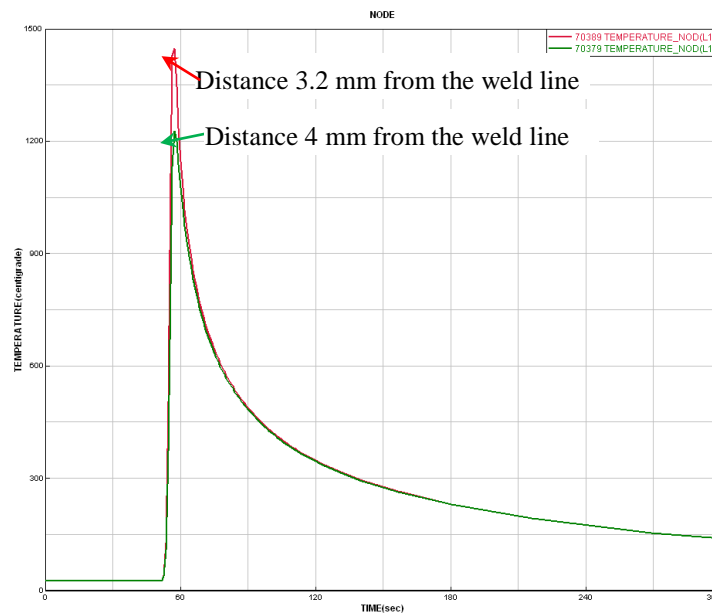


*Figure 7.* Temperature distribution at points near weld line.

Figure 7 shows the temperature cycle at the node located 0.7 mm from the weld toe (3.2 mm from the weld center). The maximum temperature of this point is 1446.5 $^\circ$C. This temperature is only slightly above the melting point. Thus, beyond this point, it is considered that the melting temperature has not been reached. It means that the fusion depth at the top surface of the weld groove is 0.7 mm. The maximum temperature at this point decreased by 392.5 $^\circ$C as compared with that at the weld toe. So, the temperature difference between the points near the weld line is very large.

The temperature cycle at the node located 4 mm from the weld line is given in Figure 7. The maximum temperature of this point is 1226.3 $^\circ$C. This temperature is much lower than the melting point of the base material.

## 4.2. Stress distribution along weld line

a) Case 1 - Without clamping
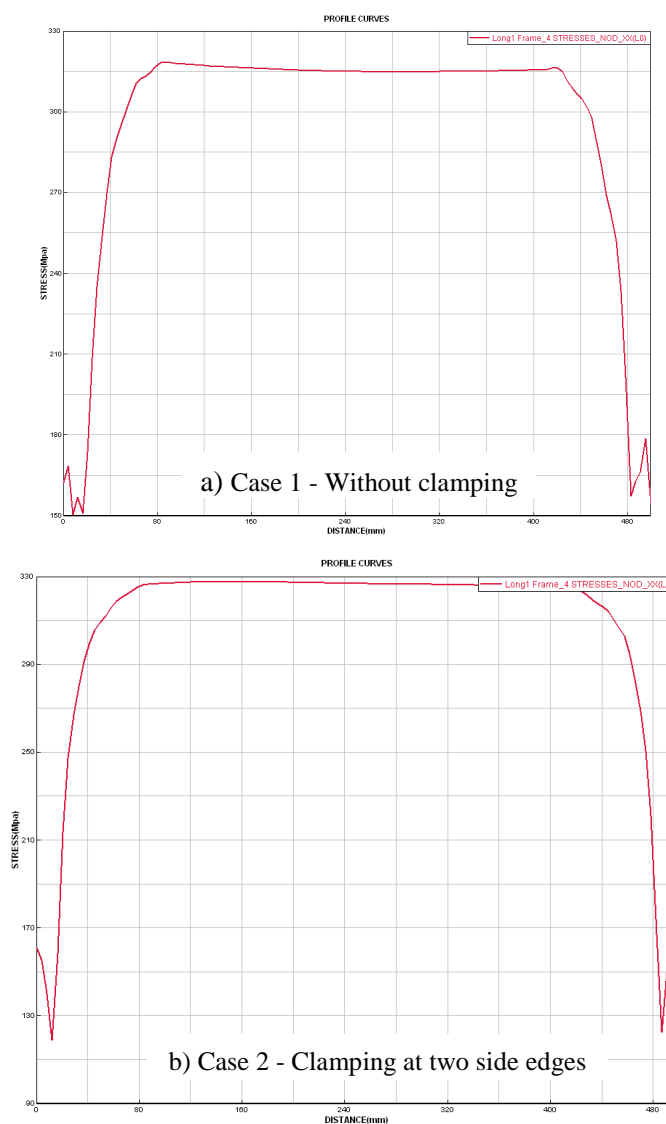
b) Case 2 - Clamping at two side edges

*Figure 8.* Longitudinal stress distribution along the weld line.

Figure 8 presents the longitudinal stress distribution ($\sigma_x$) along the weld line on the bottom surface of the plate in two cases (without and with clamping). At the start and stop end of the weld seam, the longitudinal stress is small. It is about 150 Mpa at the end of the weld seam. It rapidly increases to over 300 Mpa at 80 mm from the weld end. In the remaining region, the longitudinal stress on the weld line is almost stable. The maximum stress in the middle of the weld line in case 1 is 315 Mpa, it is 327 Mpa in case 2. This stress exceeds the yield strength of the material (= 207 Mpa), but it is still much smaller than the ultimate tensile strength of the material (= 538 Mpa). The maximum longitudinal stress on the weld line in the case of no clamping is not much greater than that in the case of clamping. This difference is only 3.8 %.

The transverse stress distribution ($\sigma_y$) along the weld line at the bottom surface of the plate in two cases (no clamping and clamping) is given in Figure 9.

a) Case 1 - Without clamping

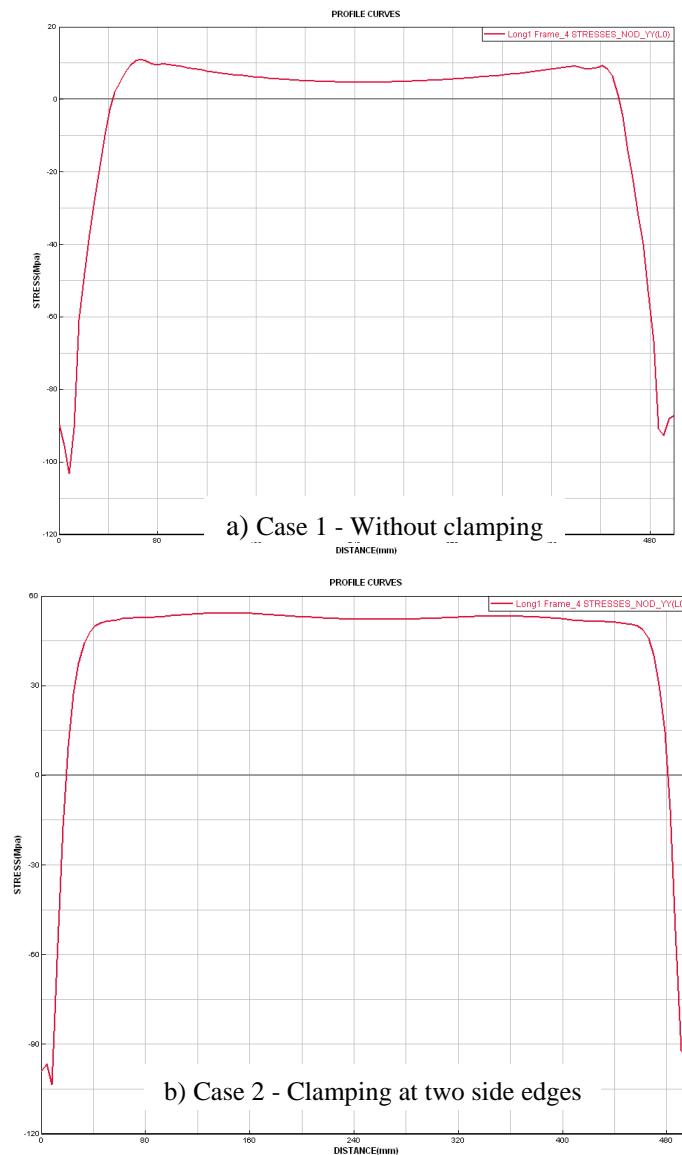b) Case 2 - Clamping at two side edges

*Figure 9.* Transverse stress distribution along the weld line.

The transverse stress distribution is in accordance with the theory: the transverse stress is compressive at the ends of weld line and tensile in the middle of weld line [11]. In the middle of weld line, the transverse stress value in the case of no claming is 4.7 Mpa. At the beginning and end of the weld, maximum compressive transverse stress in this case is -103.3 Mpa. Thus, the transverse stress at the two ends of weld line is 22 times greater than the stress in the middle of weld line. In theory, the negative stress at the two ends of weld line is only twice as large as the transverse stress in the middle of weld line. The transverse stresses at the two ends of weld line of two cases are not much different (only 0.3 %). However, the transverse stress at the middle of weld line in the case of clamping is 11 times greater than that in the case of no clamping (52 Mpa compared to 4.7 Mpa).

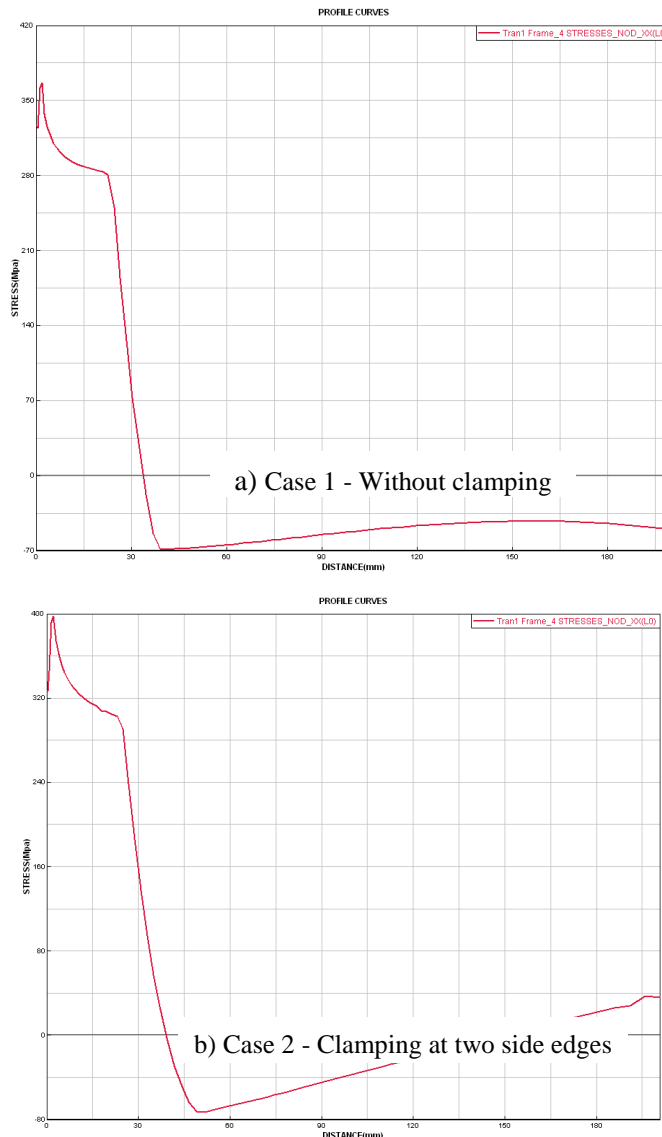### 4.3. Stress distribution from the weld line to the plate edge



a) Case 1 - Without clamping



b) Case 2 - Clamping at two side edges

*Figure 10.* Longitudinal stress distribution from the weld line to the plate edge.

Figure 10 shows the longitudinal stress distribution ($\sigma_x$) from the weld line to the plate edge on the bottom surface of the plate at the mid-length (BC line in Figure 2) in two cases. This stress distribution is consistent with the theory: the stress in the active region is tensile and it is compressive in the reactive region [11]. The maximum active stress in the case of no clamping is 366 Mpa, which is larger than the yield strength of the material (=207 Mpa). At the edge of the plate, the reactive stress in the case of no clamping is -50 Mpa. The width of the active stress zone is 33 mm.

In the case of clamping, the longitudinal active stress is 8.7 % higher than that in the case of no clamping. However, at the plate edge, in the case of clamping, the reactive stress has a positive value, in contrast to the case of no clamping, it is negative stress. The maximum compressive stress in the reactive zone in the case of clamping is 6.6 % greater than that in the case of no clamping.

## 5. CONCLUSIONS

In this study, the simulation of the MIG welding process for stainless steel materials is performed numerically by the finite element method. The three-dimensional model of the 316L stainless steel butt joint is analyzed in the SYSWELD software. The temperature field on the 316L butt joint during welding is obtained. The longitudinal and transverse residual stresses in the case of no clamping and the case of clamping are determined. From the longitudinal residual stress distribution, the dimension of the active stress zone can be calculated.

The obtained results show that the stainless steel material has good thermal conductivity, and the temperature gradient varies greatly at points near the centerline of the weld. The temperature field in the case of clamping is the same as in the case of no clamping. The maximum temperature at the point 0.7 mm from the weld toe is nearly 400 $^0$C lower than that at the weld toe.

The longitudinal stress at the middle of weld line is very high. Its value exceeds the yield strength of the material. However, the width of active stress region is small (about 35÷40 mm). The sign of stress in the active region is opposite to the sign of stress in the reactive region. When the structure is loaded, there will be a redistribution of stress: the active stress will tend to decrease. For important structures, suitable measures should be taken to reduce residual stresses. One of the simple methods that can be applied is the hammering of the weld [12]. After cooling, the weld run will be hammered following the direction of welding. The weld metal and the weld vicinity zone will be stretched and deformed plastically. Tensile residual stresses will be reduced.

The compressive transverse stress at the two ends of the weld seam is 22 times greater than the tensile transverse stress in the middle of the weld seam. The transverse stress at the ends of the weld seam in the case of clamping and the case of no clamping is not much different, but in the middle of the weld seam, the transverse stress in the case of clamping is very large, it is 11 times greater than that in the case of no clamping. Therefore, to reduce residual stress after welding, it is not recommended to use the clamps.

In the case of clamping, the longitudinal reactive stress on the line perpendicular to the weld line is divided into 2 regions: the inner region is the compressive stress, the outer region (near the plate edge) is the tensile stress. On the contrary, the longitudinal reactive stress in the case of no clamping is always compressive.

***CRediT authorship contribution statement.*** Author 1: All content of this paper.

***Declaration of competing interest.*** The authors declare that they have no known competing financial interests or personal relationships that could have appeared to influence the work reported in this paper.

## REFERENCES

1.  Ghosh N., Pal P. K., Nandi G. - Parametric optimization of MIG welding on 316L austenitic stainless steel by Taguchi method, Archives of Materials Science and Engineering, 79/1 (2016) 27-36.

2.  Jeyakumar M., Christopher T., Naraynan R., Nageswara Rao B. - Residual stress evaluation in butt-welded steel plates, Indian Journal of Engineering & Materials Sciences **18** (2011) 425-434.

3.  Lee S. H., Kim E. S., Park J. Y., Choi J. - Numerical analysis of thermal deformation and residual stress in automotive muffler by MIG welding, Journal of Computational Design and Engineering **5** (2018) 382-390.

4.  Raffaele Sepe, Alessandro De Luca, Alessandro Greco, Enrico Armentani - Numerical evaluation of temperature fields and residual stresses in butt weld joints and comparison with experimental measurements, Fatigue & Fracture of Engineering Materials & Structures **44** (2021) 182-198.

5.  Dhayanithi Venkatkumar, Durairaj Ravindran - Effect of boundary conditions on residual stresses and distortion in 316 stainless steel butt welded plate, High Temperature Materials and Processes **38** (2019) 827-836.

6.  ESI Group - Sysweld 2017 Reference manual, January 2017.

7.  John A. Goldak, Mehdi Akhlaghi - Computational welding mechanics, Springer, 2005.

8.  Nguyen N. T. - Thermal analysis of welds, WIT press, 2004.

9.  Venkata K. A., Truman C. E., Wimpory R. C., Pirling T. - Numerical simulation of three-pass TIG welding using finite element method with validation from measurements, International Journal of Pressure Vessels and Piping **164** (2017) 68-79.

10. Damian Kotecki, Frank Armao - Stainless Steels – Welding Guide, Lincoln Electric, 2003, pp. 68-79.

11. Trochun I. P. - Internal forces and deformations during welding, State Scientific and Technical Publishing House of Machine-Building Literature, Moscow, 1964 (in Russian).

12. GSI SLV Duisburg - The welding engineer's current knowledge: International Welding Engineering, 2015.